3D printing of thermoplastic polyurethane on woven fabric for body-centric applications

Abstract: Some studies have reported using 3D-printed dielectric electroactive polymer (DEAP) on woven fabric (WF) for a suitable electroactive response in the past decade. However, little has been reported on using 3D-printed thermoplastic polyurethane (TPU) on WF as a part of a wearable sensor in body-centric applications (BCA). This study reports the effect of mechanical loading (0-25N) on the dielectric constant (ε_r) of 3D-printed TPU over WF as a substrate for BCA. For ascertaining the change in ε_r, the substrate was loaded and unloaded (for repeated cycles) along the weft side of the WF for mechanical strain. The 3D printed TPU on WF has shown programmable changes as 4D capabilities in bond characteristics (based on attenuated total reflectance-Fourier transform infrared (ATR-FTIR), surface roughness (R_a), porosity % (based on scanning electron microscopy (SEM), and physical properties (based on X-ray diffractions (XRD) analysis). To ascertain the BCA, the wearability of the developed sensor was ensured based on the specific absorption rate (SAR), which was observed as 1.57W/kg.

Keywords: Electroactive polymer; 4D characteristics; wearable sensor; body centric applications; TPU

TPU is one of the flexible 3D printable materials used in fused filament fabrication (FFF), and it has shown applications in actuators, sensors [1], and energy harvesters [2]. Some studies have reported using FFF to print substrates for patch antennas using recycled thermoplastics [3]. Also, 3D printing in textile printing has opened many possibilities for smart clothing and wearable sensors [4]. Researchers have successfully printed polymers on WF using FFF [4, 5]. The reported literature has outlined that moisture, pH value, magnetic, electric field, temperature, light, etc., may be stimuli for 4D capabilities [6, 7]. In the past decade, TPU, a DEAP, has been used as a scaffold for biomedical applications. Also, some studies have reported using 3D-printed TPU on WF to enhance electroactive responses. But hitherto, little has been reported on 3D-printed TPU on WF as a wearable sensor in BCA with 4D capabilities. This study reports the effect of mechanical loading (0-25N) on ε_r of 3D printed TPU over WF (cotton on the warp side and lycra on the weft side) as a substrate for ensuring BCA.

For ascertaining the change in ε_r, the substrate was loaded and unloaded (for 03 cycles) along the weft side of the WF to ensure the mechanical strain. Fig.1 shows the methodology adopted in this study. The virgin TPU used in this study has a melt flow index (MFI) of 29.758 g/ (10 min). The WF was stretchable along the weft side to provide the required strain to the substrate. TPU substrate was printed on unstrained WF at 225°C nozzle temperature, 60°C bed temperature, 18mm/s printing speed, and an infill density of 60%. The pilot study shows the change of ε_r and loss tangent (tanδ) based on the ring resonator technique (for the substrate of 60×54×0.65 mm) from 1.74-2.07 and 0.0047-0.0049, respectively, with load application from 0-25N [3]. For a ring, feed lines, and ground plane, Cu tape (thickness 0.08 mm) was used.

The bond characteristics of 3D printed samples were studied using ATR-FTIR for three cycles of loading and unloading (Fig. 2a-c), which shows the peak at 2927cm^{-1} (attributed to stretching of -CH bond), whereas peaks at 2356cm^{-1} and 2322cm^{-1} attributes to CO_2 stretching. The peak at 1728cm^{-1} represents the presence of the -C=O bond, and 1526cm^{-1} shows the presence of -N-H deformations indicating the urethane structure. A peak at 1596cm^{-1} may be ascribed to atomic -C=C- stretching vibrations, and the peaks at 1728cm^{-1} and 1699cm^{-1} represent stretching vibrations of carbonyl groups, whereas bonds can be attributed to easter and urethane carbonyl, respectively. The peaks at 1300cm^{-1} to 1100cm^{-1} spectral region are assigned to C-O stretching vibrations of urethane units or C-O stretching vibrations of esters [8, 9]. It was observed that the absorbance value for peaks for a loaded substrate was more than the unloaded one, and repetition was shown in three cycles, which confirms its two-way programmability for 4D characteristics. Fig. 2(d) shows the XRD spectrum of samples under loaded and unloaded conditions. Peaks at 10° and 20° justify the existence of -NH_2 and -OH groups, respectively [10]. It was observed that there was an increment in the intensity when the sample was loaded compared to the unloaded, which may be because of the higher concentration of the atoms.

Further, a patch antenna (as a sensor) was designed for a 2.45GHz resonating frequency as per the literature [3]. The calculated dimensions are shown in Fig. 3a. The simulation was performed using high-frequency simulation software (HFSS), which shows the antenna resonation at 2.45 GHz, but the SAR value was very high, 4.450 W/kg (Fig.3b-c). SAR value can be reduced for an operating frequency of 2.4 GHz by changes in patch shape, size, ground plane design, use of metamaterials, slotting of the patch, use of high permittivity substrates, impedance matching, balanced feeding and using different optimization algorithms etc. For addressing this issue, the patch was cut at the various sections with low electric field areas, and the designed patch with dimensions is shown in Fig. 3d. The simulation indicates that the sensor now is resonating at 3.10 GHz and 5.30 GHz (Fig.3e) which lies in Wi-Fi range and SAR value was reduced to 1.57 W/kg over 1g of body tissue (Fig.3f) which lies within a permissible limit; hence the purposed 3D printed DEAP on fabric may be used for body-centric applications.

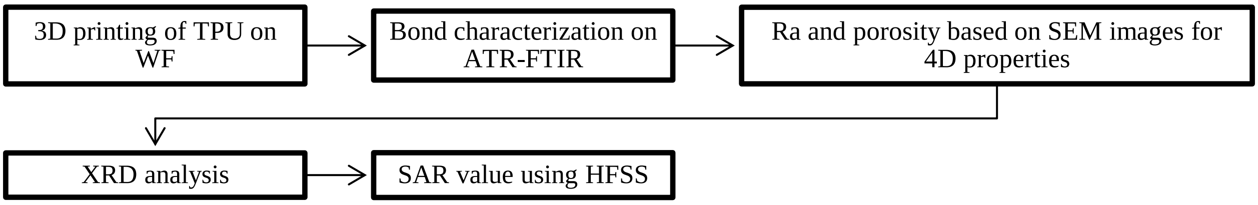

Fig.1: Methodology used in present work

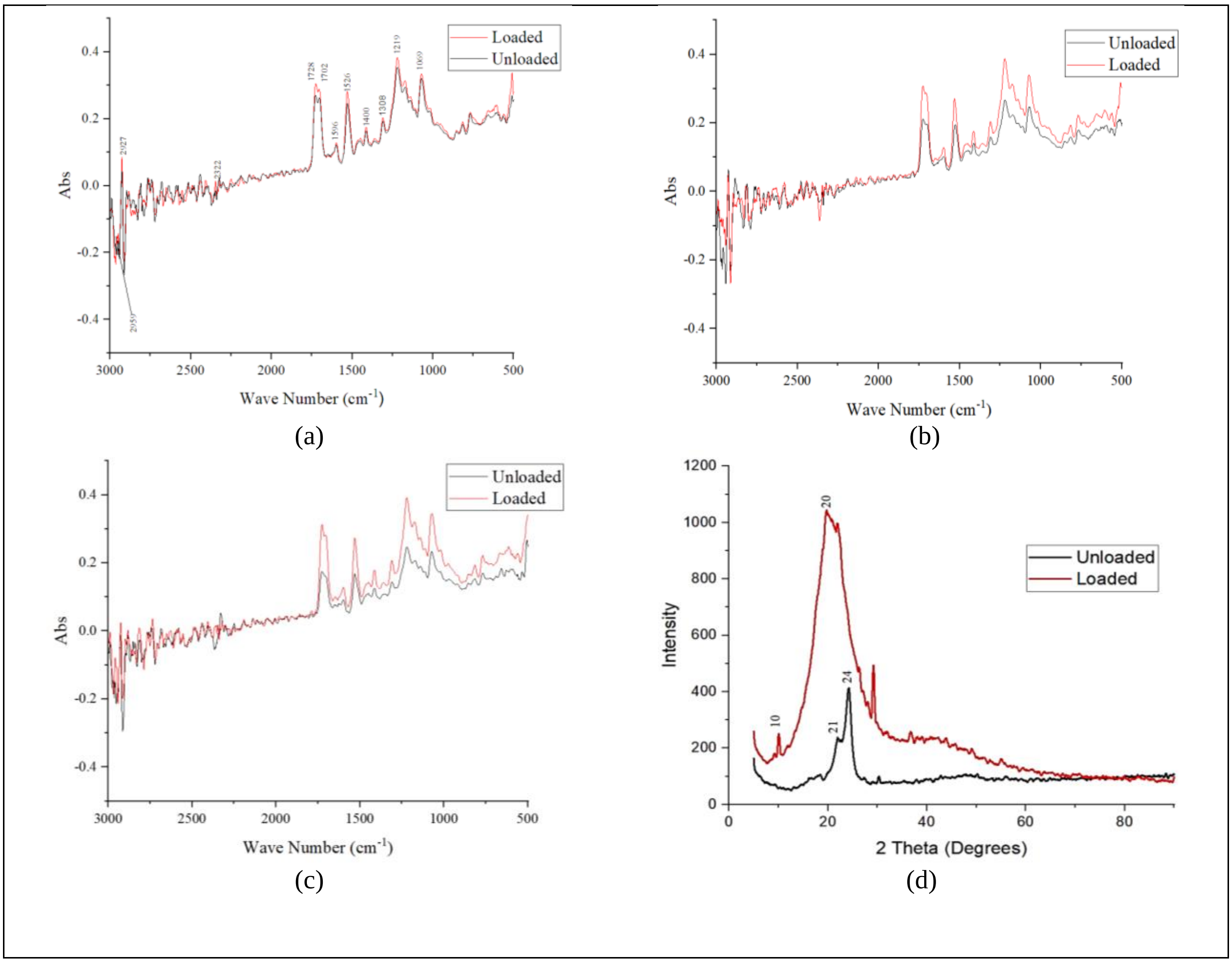

Fig. 2: ATR-FTIR spectrum (a) first cycle, (b) second cycle, (c) third cycle, (d) XRD spectrum under loaded and unloaded condition

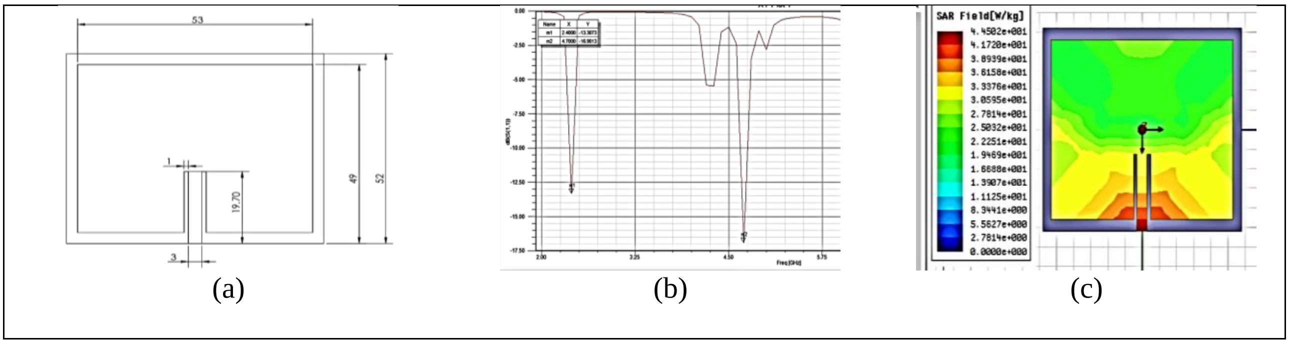

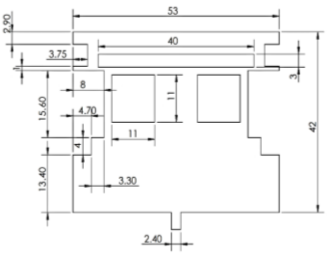

(d)

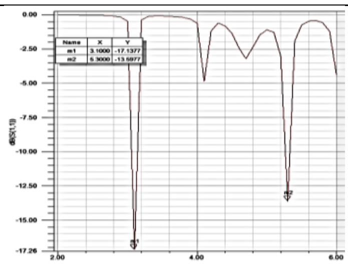

(e)

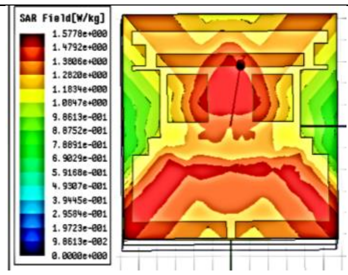

(f)

Cycle 1 (Un-loaded sample)

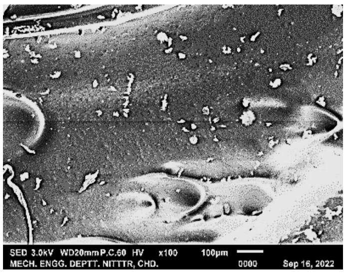

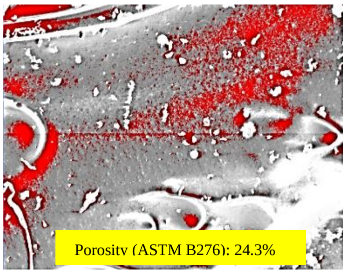

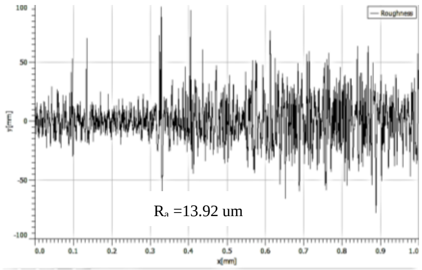

Cycle 1 (Loaded sample)

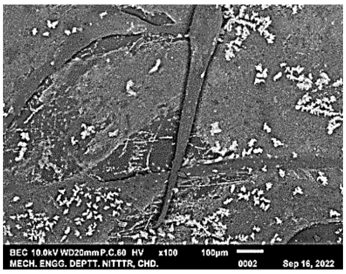

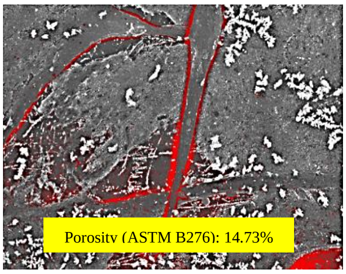

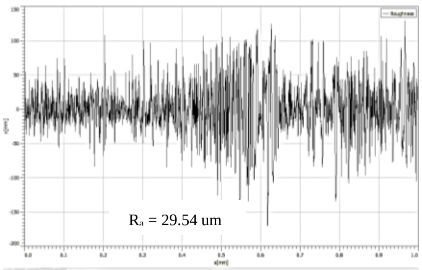

Cycle 2 (Un-loaded sample)

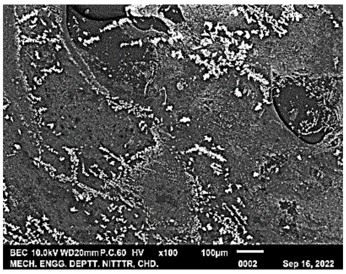

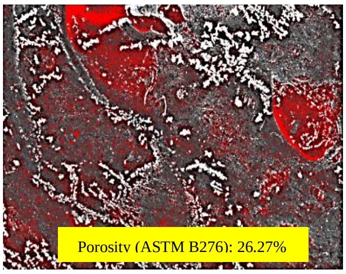

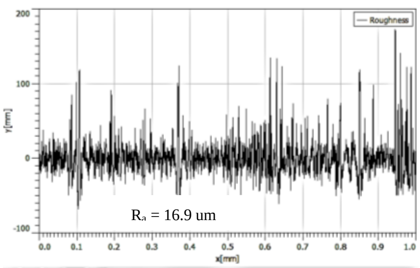

Cycle 2 (Loaded sample)

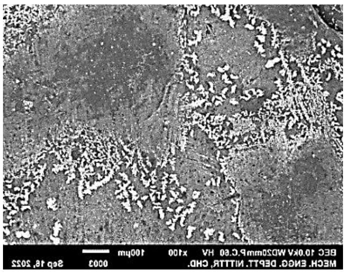

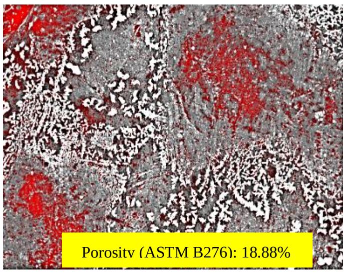

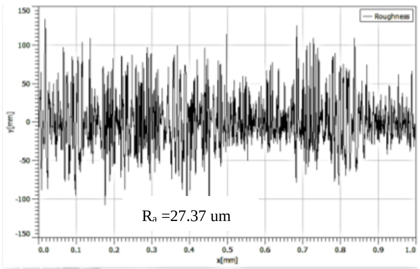

Cycle 3 (Un-loaded sample)

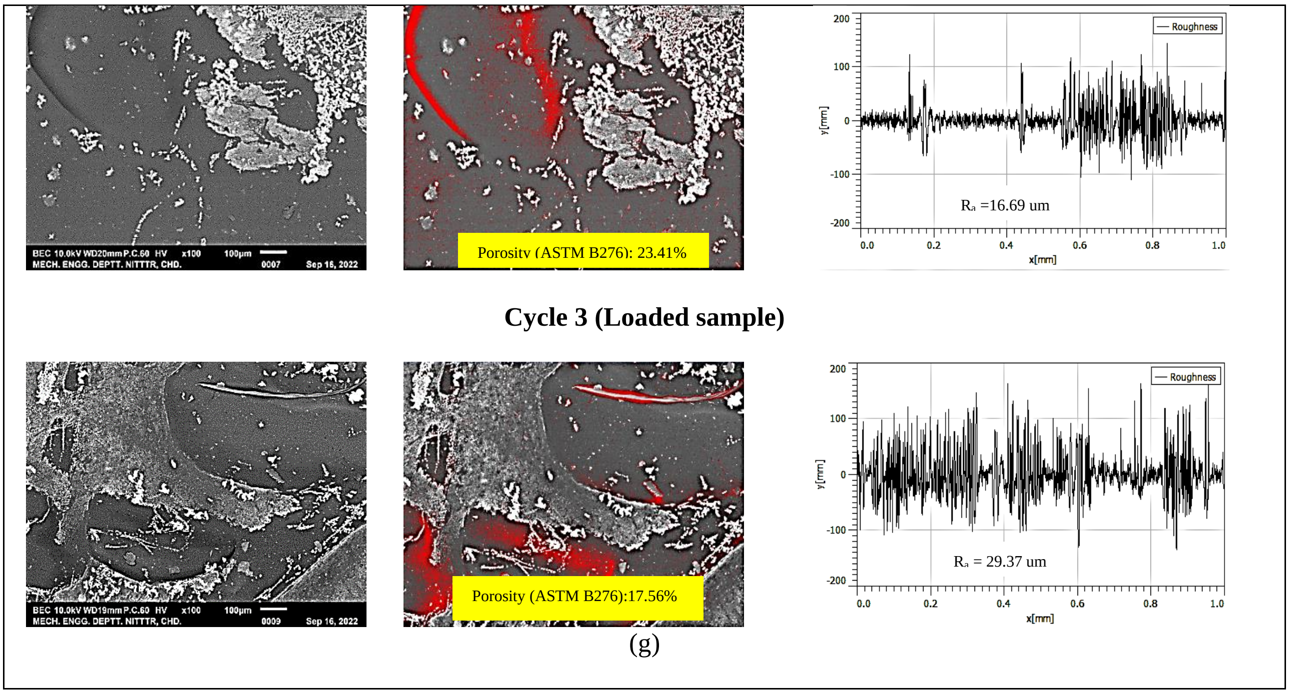

Fig. 3: Patch calculated dimensions (a), Observation for resonance frequency (b), SAR value observation (c), modified designed patch (d), resonance frequency observation with a modified patch (e), SAR value with a modified patch (f), SEM images, Porosity%, R_a for different loading and unloading cycles (g)

Note: The loading of samples resulted in porosity % reduction because of the overlapping of strands of WF.

The SEM images of samples were captured for 03 cycles (for calculating porosity% and surface roughness (R_a) profiles) (Fig.3g), which shows that for cycle 01, the unloaded sample has a porosity of 24.3%, whereas a loaded sample has 14.73%. For cycle 02, it was 26.27% for unloaded and 18.88% for loaded samples. For cycle 3, porosity was 23.41% in unloaded and 17.56% in loaded condition. The R_a for a sample were 13.92um and 29.54um for unloaded and loaded conditions, respectively (in cycle 01); again on unloading the sample, the R_a decreased to 16.9um and increased on loading 27.37um (cycle 02), and in cycle 03, R_a followed the same pattern 16.9um and 29um for unloaded and loaded condition respectively. It was observed that the porosity and R_a have also shown repeatability in the results under loading and unloading conditions, ascertaining the 4D characteristics. Hence, 3D-printed TPU (selected as DEAP in the present case study) over WF may enhance the electroactive responses of sensing applications.

References:

1. Bar-Cohen Y, Cardoso VF, Ribeiro C et al (2017) Electroactive polymers as actuators. In: Uchino K (ed) Advanced piezoelectric materials, 2nd edn. Woodhead Publishing, UK, pp 319-352
2. Singh T, Kumar S, Sehgal S (2020) 3D printing of engineering materials: A state of the art review. Material Today Proc. 28:1927-1931
3. Singh R, Singh BP, Singh AP et al (2022) Effect of Infill Density on the Performance of Recycled PET-Based 3D Printed Microstrip Antenna. National Academy Science Letters 45:525-529
4. Spahiu T, Al-Arabiyat M, Martens Y et al (2018) Adhesion of 3D printing polymers on textile fabrics for garment production. IOP Conf. Ser.: Mater Sci and Eng. 459: 012065
5. Pei E, Shen J, Watling J (2015) Direct 3D printing of polymers onto textiles: experimental studies and applications. Rapid Prototyping J 21: 556-571
6. Schmidt AM (2006) Electromagnetic activation of shape memory polymer networks containing magnetic nanoparticles. Macromolecular Rapid Communications 27:1168-1172
7. Ly ST, Kim JY (2017) 4D printing–fused deposition modeling printing with thermal-responsive shape memory polymers. Int J of Precision Engineering and Manufacturing-Green Technology 4:267-272
8. Nadgorny M, Ameli A (2018) Functional polymers and nanocomposites for 3D printing of smart structures and devices. ACS applied materials and interfaces 10:17489-17507
9. Bruckmoser K, Resch K (2014) Investigation of ageing mechanisms in thermoplastic polyurethanes by means of IR and Raman spectroscopy. Macromol. Symp. 339: 70-83

10. Amjed N, Bhatti IA, Simon L et al (2022) Preparation and characterization of thermoplastic polyurethanes blended with chitosan and starch processed through extrusion. Int J of Biological Macromolecules 208:37-44